Nanomanufacturing and Metrology (2023) 6:34
https://doi.org/10.1007/s41871-023-00214-5

ORIGINAL ARTICLE

HG-Induced sEVs Mediate Biomechanics of HK-2 Cells

Fan Yang[1,2,3] · Jiajia Wang[1,2] · Tuoyu Ju[1,2,3] · Shuwei Wang[4] · Kaige Qu[1,2,5] · Zhengxun Song[1,2,3] · Yujuan Chen[1,2,3] · Zuobin Wang[1,2,3,5]

Received: 30 June 2023 / Revised: 1 September 2023 / Accepted: 4 September 2023

Abstract

Small extracellular vesicles (sEVs) participate in the pathological progression of high glucose (HG)-induced kidney injury, which is closely related to diabetic nephropathy. How sEVs specifically mediate the cell biomechanics underlying HG injury is unclear. Herein, we utilized a versatile atomic force microscope to determine the contributions of sEVs in HG-induced cellular injury. The sEVs extracted from the culture medium of human proximal tubule kidney (HK-2) cells treated by HG for 72 h (HG-induced sEVs) were verified and analyzed by multiple techniques, and the results indicated the effective production and the effect of dehydration on the shape of HG-induced sEVs. Further investigation on the morphologies of HK-2 cells treated by HG-induced sEVs showed that the surface roughness of the HK-2 cells increased, and their pseudopodia transitioned from lamellipodia to filopodia, with almost doubled mean pseudopodia length. Quantitative analysis of the mechanical responses of the cells revealed that the mean Young's modulus increased by 26.2%, and the mean adhesion decreased by 36.8%. The indirect mediation of cellular biomechanics guided by HG-induced sEVs was evaluated by comparing it with previously studied direct HG injury. The HG-induced sEVs caused a greater reduction in cell adhesion and an increase in Young's modulus compared with direct HG stimulation. This work suggested the ability of HG-induced sEVs to elicit specific biomechanical responses during HG injury, advancing the understanding of the injury mechanism caused by HG. The comparison of the cellular biomechanics between direct and indirect HG stimulations through HG-induced sEVs can be beneficial for the diagnosis and treatment of kidney injury.

Highlights

1. AFM characterized the morphology of HG-induced sEVs with nanometer resolution and revealed the effect of dehydration on their shapes.
2. High-resolution and quantitative biomechanical characterization of living HK-2 cells confirmed that HG-induced sEVs mediate the biomechanics of HK-2 cells, suggesting the underlying role of sEVs during HG injury.
3. The AFM-based biomechanics of HK-2 cells serve as promising biomarkers for assessing the differences between direct HG stimulation and indirect HG stimulation through HG-induced sEVs.

Keywords AFM · Cellular biomechanics · HG-induced sEVs · HG · HK-2 cells

✉ Yujuan Chen
chenyujuan@cust.edu.cn

✉ Zuobin Wang
1561788492@qq.com

[1] International Research Centre for Nano Handling and Manufacturing of China, Changchun University of Science and Technology, Changchun 130022, China

[2] Centre for Opto/Bio-Nano Measurement and Manufacturing, Zhongshan Institute of Changchun University of Science and Technology, Zhongshan 528437, China

[3] Ministry of Education Key Laboratory for Cross-Scale Micro and Nano Manufacturing, Changchun University of Science and Technology, Changchun 130022, China

[4] Affiliated Hospital, Jilin Medical University, Jilin 132013, China

[5] JR3CN & IRAC, University of Bedfordshire, Luton LU1 3JU, UK

Published online: 18 September 2023

1 Introduction

Small extracellular vesicles (sEVs), including exosomes, are generally nanometer in size (30–150 nm) and carry rich biological substances such as lipids, proteins, and nucleic acids [1–5]. These cell-derived vesicles could implement crosstalks between parental and recipient cells and trigger specific cell responses. This unique ability of sEVs recently aroused huge interest and was proven to be involved in the pathogenesis of various diseases, such as cancers [6–8], inflammations [9–11], metabolic disorders [12], and diabetes and its complications [13–16]. Regarding the mechanism of diabetic nephropathy (DN), it is already clear that direct high glucose (HG) stimulation could damage the filtering system inside the kidney and cause kidney injury [17–21]. However, the contribution of sEVs in this injury progression remains to be determined.

To our knowledge, much effort has been directed to figure out the participation of sEVs in kidney injury [22–25]. Wu et al. [26] validated the promoting effect of exosomes on renal fibrosis and confirmed that exosomes affected epithelial–mesenchymal transition (EMT) and renal fibrosis in DN via the paracrine communication between specific cells [27]. TGF-β1 mRNA, a genetic molecule involved in EMT and fibrosis, is transported by exosomes from injured epithelial cells to activate the fibroblasts [28]. So far, most of these findings were obtained using biological methods and were based on cell population experiments.

Recent encouraging studies showed that sEVs could regulate the biomechanics of cells [29] and even tissues [6]. For kidney fibrosis, cell biomechanics are potential markers at the single-cell level [30–34]. The elasticity and adhesion of tubular cells in vivo are closely related to fibrosis and injury processes [35]. With the use of an atomic force microscope (AFM), the increase in cellular stiffness of NRK52E cells has been identified as a sign of cellular fibrosis [36]. According to the AFM results, the EMT process could be characterized by analyzing the structural changes of cells [37]. In our previous study, the dynamic injury of human proximal tubule kidney (HK-2) cells caused by direct HG stimulation was quantitatively characterized by AFM mapping [38]. Formerly referred to as exosomes according to the MISEV guidelines, sEVs could also be characterized by high-resolution AFM [39]. These results inspired us to further explore the regulation of cell biomechanics by sEVs under indirect HG-induced kidney injury.

In this study, HG-induced sEVs were extracted to stimulate normal HK-2 cells, as shown in Fig. 1A. The

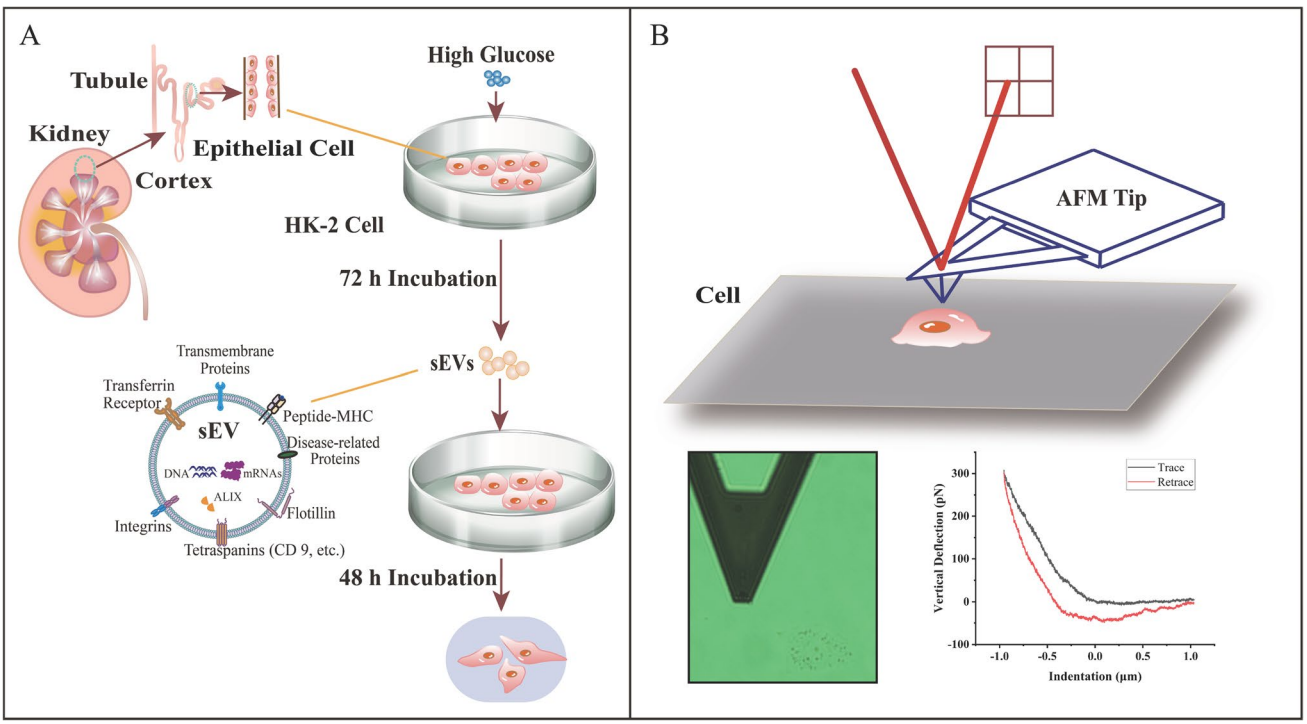

Fig. 1 Illustration of HG-induced sEVs regulating the biomechanics of HK-2 cells. **A** Protocol of HG-induced sEVs mediated by indirect HG treatment. HK-2 cell is a cell model for kidney research. The biological structure and contents of a sEV are also shown. **B** AFM-based characterization of HK-2 cells, with an optical image of AFM scanning and a typical force–distance (FD) curve

biomechanical responses of HK-2 cells to different concentrations of HG-induced sEVs were then examined by AFM in liquid and air as shown in Fig. 1B. Finally, the effects of HG-induced sEVs were compared with those of direct HG injury to help confirm and understand the role of HG-induced sEVs during HG injury and to provide insights into sEV-based therapeutic approaches for the diagnosis and treatment of kidney injury.

2 Materials and methods

2.1 Cell culture and treatments.

HK-2 cells were cultured as described in Ref. [38], seeded in 90 mm dishes, and exposed to HG (60 mmol/L) for 72 h after reaching a confluence of 80%. The treatment duration and HG concentration were consistent with the HG conditions reported in Ref. [38] to ensure the induction of cell injury. HG-induced sEVs were collected from the culture mediums of the parental cells, that is, the pretreated HK-2 cells. The untreated HK-2 cells were labeled as the recipient cells; cultured in fresh minimum essential medium with basal glucose (5 mmol/L), 10% EV-depleted FBS (ABW), and different concentrations of HG-induced sEVs (0, 500, 1000, and 2000 μg/mL) for 48 h, and named as HK-2-N, HK-2-E_{500}, HK-2-E_{1000}, and HK-2-E_{2000}, respectively.

2.2 Extraction of HG-induced sEVs

The supernatants of HK-2 cells treated with HG for 72 h were collected, centrifuged at 2000 × *g* for 10 min, recentrifuged at 10,000 × *g* for 30 min, filtered with 0.22 μm pore filters (Millpore), and ultracentrifuged (Beckman Coulter, Optima XE-90, USA) at 100,000 × *g* for 70 min. After the supernatant was removed and resuspended with PBS, a second ultracentrifugation was applied with the same parameters. The HG-induced sEVs were extracted, stored at − 80 °C, and examined with a BCA kit (Sangon Biotech).

2.3 Western blot (WB) for HG-induced sEV markers

Lysates of HG-induced sEV extractions were separated by 10% SDS-PAGE, and the proteins were transferred onto a PVDF membrane. After blocking by BSA solution, the membrane was first incubated separately with the mouse polyclonal antibody for CD9 and ALIX, followed by anti-mouse secondary antibodies. Finally, the protein markers of HG-induced sEVs were imaged with the imaging system (Analytik Jena, ChemStudio SA2, Germany) after hypersensitive chemiluminescence.

2.4 AFM characterization of HK-2 cells and HG-induced sEVs

The cells and HG-induced sEVs were characterized by AFM (JPK, Nano Wizard 3, Germany). The living cells, plated on cover glasses in Petri dishes, were investigated under the Quantitative Imaging Mode in liquid using an MLCT cantilever (Bruker, Spring Constant: 0.07 N/m) with the setpoint of 1 nN. The force curves of each pixel and the quantitative images were recorded. At least 10 cells were detected for each sample, and the detection was repeated three times. Hertz fitting was applied to calculate the Young's modulus of cells.

The HG-induced sEVs, diluted appropriately and drop-casted on the mica, were imaged under the tapping mode in the air using a Tap300Al-G cantilever (Budget Sensors, Spring Constant: 40 N/m) with the setpoint of 2 nN. All the AFM results were processed with the JPK data processing software.

2.5 Scanning electron microscopy (SEM) imaging of HG-induced sEVs

In brief, 5 μL of the diluted HG-induced sEVs was dropped onto the silicon substrates, followed by a drop of 4% glutaraldehyde for fixation. The HG-induced sEVs were dried and then coated with a thin golden film of 1 nm thickness. The HG-induced sEVs were imaged by SEM (FEI, Helios G4 CX, USA).

3 Results and discussion

3.1 Characterization of HG-induced sEVs

Multiple techniques were applied to determine the HG-induced sEV features, such as particle size, distribution, and morphology. High-resolution images of HG-induced sEVs were produced via SEM and AFM. The individual HG-induced sEVs displayed an approximate sphere shape with a diameter of about 90 nm in Fig. 2A. Meanwhile, the HG-induced sEV populations were observed by AFM in a wide range (Fig. 2B) for the mathematical determination of the size distribution. Five AFM images were chosen for plotting the diagram. The histogram showed a unimodal size distribution of the HG-induced sEVs through Gaussian fitting, where 85.7% of the particles were statistically counted to exhibit lateral diameters ranging from 30 to 150 nm (Fig. 2C). The sEV-associated proteins could be specifically identified by WB experiments. The transmembrane proteins (CD9) and cytosolic proteins (ALIX) were

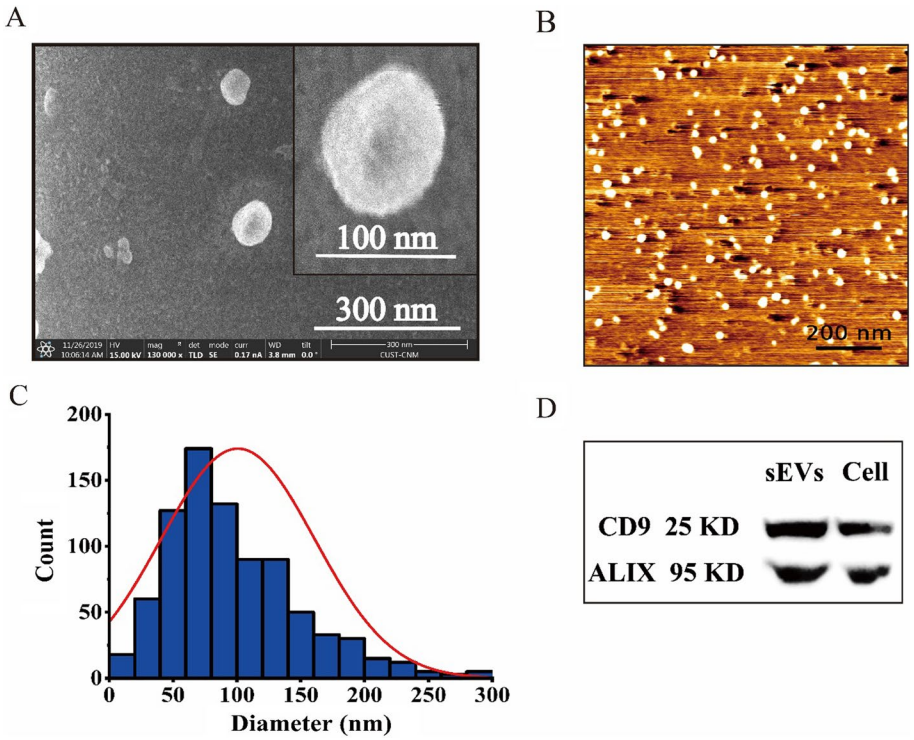

Fig. 2 Characterization of HG-induced sEVs. **A** SEM image of HG-induced sEVs. **B** AFM image of HG-induced sEVs. **C** Size distribution of the lateral diameters of HG-induced sEVs statistically calculated from the AFM topography images. **D** Western blot results of the protein markers of HG-induced sEVs, CD9, and ALIX

expressed and differentiated between the sEVs and cells (Fig. 2D).

Different from SEM, only simple preparation was required for the AFM experiment. In addition, AFM could provide 3D information for the HG-induced sEVs. In Fig. 3A, B, the HG-induced sEVs showed round shapes similar to those in the SEM images. However, the height values were relatively lower than the lateral diameters (30–150 nm), not exceeding 10 nm. A large ratio of diameter/height ($Ratio_{D/H}$) was observed (Fig. 3D), indicating the nonspecific flattening of the sEV structures. The differences in the images of sEVs are highly related to the methods of sample preparation and imaging techniques [40, 41]. The HG-induced sEV samples were adsorbed onto mica, detected in air, and might have experienced slight dehydration, thus leading to flattening.

The central areas of HG-induced sEVs were darker than the peripheries in the phase image (Fig. 3G, H), leading to the cupped shape shown in the cross-section lines (d, e) in Fig. 3I, J. However, this unique feature cannot be identified in the height image. Therefore, this collapse was not topographical but viscoelasticity-related. sEV could be described as a soft internal cavity restricted by a stiff membrane with diverse membrane components, as shown in Fig. 1A [2]. These surface molecules, such as proteins and lipids, would bind with the AFM tips. Thus, the surface viscoelasticity of HG-induced sEVs was potentially reflected in the phase images.

3.2 HG-induced sEVs activated the morphological alterations of HK-2 cells

The biomechanics of the HK-2 cells treated with increasing concentrations of HG-induced sEVs were studied by AFM to examine the role of sEVs in HG-injured kidney tubular epithelial cells. Cellular morphological features considered important markers for cellular states, such as cell shapes, pseudopodia, and surface topographies, were detected [42, 43].

The AFM images (Fig. 4A) showed that the HK-2 cells experienced dynamic shape alterations, from the original cobblestone-like shape to irregular shapes, and were ultimately elongated. The ellipticity of normal HK-2-N cells was $32.63\% \pm 13.24\%$. Meanwhile, the HG-induced sEVs increased the cell ellipticities, presenting a dose-dependent effect (Fig. 4C1). In addition, the sEVs induced the transitions of pseudopodia in their states and lengths. The ultrastructures of pseudopodia were observed, with the enlargement of detailed images marked with white squares shown in Fig. 4B. Normal HK-2 cells presented the flake-shaped pseudopodia, called lamellipodia, which extended from the cell body and the average length of 5.9 ± 1.8 µm. After the treatment of HG-induced sEVs for 48 h, the scattering lamellipodia around the cell body turned out to be filopodia, which were extended from the cells. The average lengths of pseudopodia increased with the concentrations of HG-induced sEVs (Fig. 4C2). The filopodia of HK-2-E_{2000}

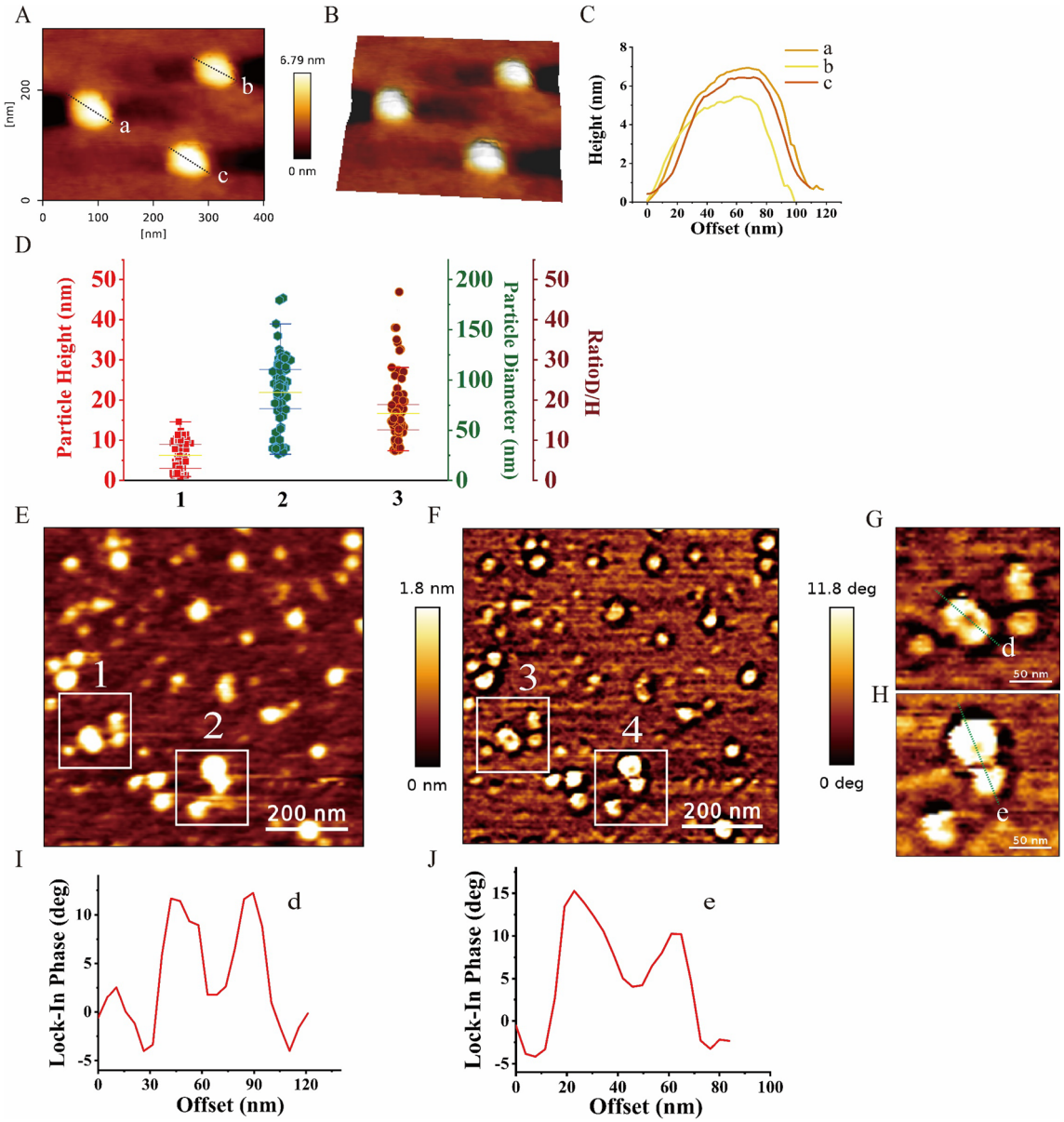

Fig. 3 Dimensional analysis of HG-induced sEVs. **A** Height image of HG-induced sEVs. **B** 3D image of HG-induced sEVs. **C** Corresponding cross-section lines of a, b, and c in **A**. **D** Particle height, diameter (lateral), and ratio of diameter/height ($Ratio_{D/H}$) of HG-induced sEVs. **E** Height image of HG-induced sEVs. **F** Phase image of HG-induced sEVs. Squares 1 and 2 are the height images, and squares 3 and 4 are the corresponding phase images of the same area. **G** and **H** Magnified phase images of squares 3 and 4. **I** and **J** Corresponding cross-section lines d and e in **G** and **H**

stretched, and the average length doubled compared with that of HK-2-N. Pseudopodia are functional components based on the microtubular cytoskeleton outgrowths of cells [44] and are involved in multiple processes, such as cell spreading, migration, and interactions between cells and external environments. Therefore, the morphologies of pseudopodia are crucial cues for characterizing the cytoskeleton dynamics.

The areas of interest with equal size ($9.4 \times 9.4\ \mu m^2$) on the cellular surfaces of individual HK-2 cells from each sample were selected as shown in Fig. S1. Compared with that of control HK-2 cells, the roughness value showed an overall increase and was maximized when the concentration of HG-induced sEVs reached 1000 μg/mL. This trend was consistent with the 3D images. Surface roughness was used as an indicator of membrane micro-irregularities [45].

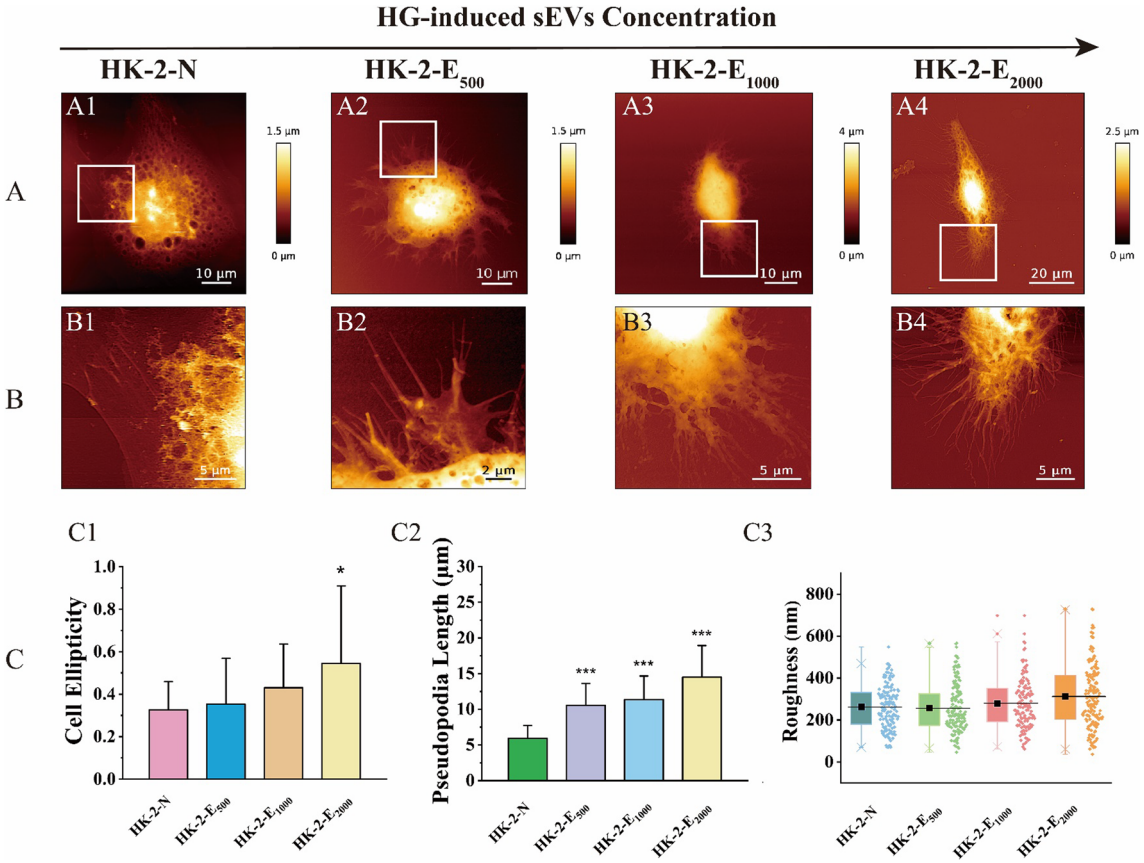

Fig. 4 Morphological transition of HK-2 cells caused by HG-induced sEVs. **A1**–**A4** AFM images of HK-2-N, HK-2-E_{500}, HK-2-E_{1000}, and HK-2-E_{2000} in air. **B1**–**B4** Corresponding zoom-in images of pseudopodia marked squares in **A1**–**A4**. **C1**–**C3** Cell ellipticity, pseudopodia length, and surface roughness. The data in **C1** and **C2** are presented as mean value ± standard deviation ($0.01 < *p < 0.05$, $0.001 < **p < 0.01$, $***p < 0.001$)

The changes in roughness suggested the surface modification caused by the interaction between the external sEVs and cells.

Moreover, the average roughness (Ra) values of at least 20 cells from each sample were plotted (Fig. 4C3) and statistically analyzed. The Ra values showed a wide range, suggesting that part of the cells exhibited increased surface roughness due to the treatments of HG-induced sEVs. A slight uptrend was observed in the average roughness in contrast with the Ra of untreated HK-2 cells. The roughness of individual cells and the average for multiple cells were increased in general, demonstrating the roughening responses of the HK-2 cells to the HG-induced sEVs. However, the concentration of HG-induced sEVs that led to the maximum roughness was inconsistent. This phenomenon could be caused by the heterogeneity of cells and the existing differences between individual cell and population analyses [46], suggesting the necessity of further analyzing the morphologies of individual cells and cell groups.

Multiple studies have concluded that HG prompted the morphological phenotype change of HK-2 cells from an oval shape to a spindle shape similar to a fibroblast [47, 48]. Our previous study was in agreement with these results [38]. In the current work, the HG-induced sEVs were derived from the HG-treated HK-2 cells, causing similar morphological conversions of HK-2 cells. The high concentration of HG-induced sEVs drove the changes in cellular shapes and pseudopodia and roughened the cellular surface to some extent. As a result, the effect of sEVs on HG-induced cellular injury was confirmed.

3.3 Quantitative analysis of cellular biomechanics affected by HG-induced sEVs

AFM allowed the quantitative analysis of the mechanical properties of living cells in their physiologically relevant liquid [49]. During the measurement, the interaction between AFM tips and cells was recorded as the FD curves to show

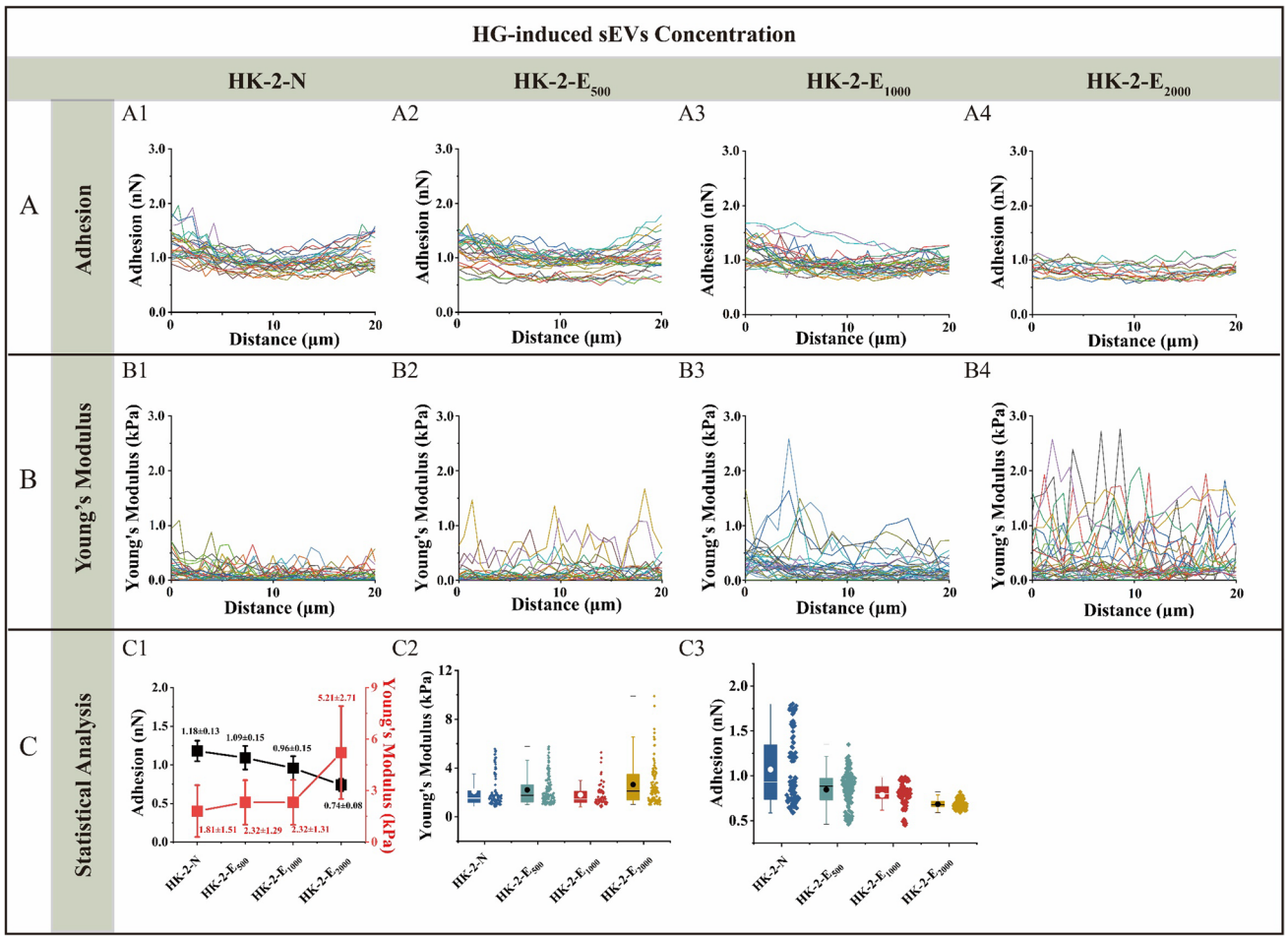

Fig. 5 Quantitative analysis of the biomechanics of HK-2 cells treated with different concentrations of HG-induced sEVs. **A1**–**A4** and **B1**–**B4** Cross-section lines from the images of adhesion and Young's modulus. The central areas of 20 cells were selected from each group. **C1** Analysis of Young's moduli and adhesions based on a single cell. **C2** and **C3** Data distributions of Young's moduli and adhesions based on cell population

the different features that depend on the sample characteristics. In general, the up-and-down motion of the probe would be inevitably resisted by liquid, leading to the distance between the extend and retract curves. Many zig–zag peaks in the retract curves were produced because of the interactions between the tips and glycocalyx coated on the cell surface. The maximum zig–zag peak was defined as the adhesion of this point. Hysteresis between the extend and retract curves was frequently found when scanning the biological samples [42].

The features of cells could be reflected by the FD curves, so their mechanical properties could be extracted from these curves [20]. Here, single-cell and multicell average analyses [50] were adopted for the quantitative evaluation of cellular biomechanics. Through the analyses of cross-section lines of Young's modulus and adhesion from the central areas of 20 cells in each group, the quantitative changes in cellular biomechanics were observed, as shown in Fig. 5A and B. With the increasing concentrations of HG-induced sEVs, Young's modulus increased, and adhesion decreased.

Young's modulus and adhesion were two crucial parameters for characterizing biomechanics, with the former derived from the fitting mathematical models of contact mechanics and the latter directly obtained from the FD curves. The Hertz model was the simplest and most used contact mechanics model for calculating the elasticity of living cells [51–53]. Although it did not take surface adhesion into account, it was still an effective one-parameter model and was suitable for the relative quantifications because the varying adhesions of the cellular surface would lead to a high level of inaccuracy. The Young's modulus and adhesion for a single cell are shown in Fig. 5C1.

Young's moduli and adhesions were box-plotted in Fig. 5C2 and C3. Multicell level analysis revealed the general mechanical changes of HK-2 cells responding to the different concentrations of HG-induced sEVs. The Young's moduli of HK-2-E_{500} and HK-2-E_{1000} showed minor differences to those of HK-2-N. Only partial cells from HK-2-E_{2000} displayed sharply increased Young's moduli. The adhesion showed a downward tendency and was remarkably reduced with the increasing sEV concentrations.

The mechanical properties were found to be related to the concentrations of the HG-induced sEVs. At the maximum concentration of 2000 μg/mL, the cellular biomechanics exhibited differences. In particular, the HG-induced sEVs affected the cellular surface adhesion more than Young's modulus because only a few HK-2 cells showed sharply increased Young's moduli. The average Young's modulus increased by 26.2%, and the average surface adhesion decreased by 36.8% (from 1.071 to 0.685 nN).

The elasticity and surface adhesion were tightly linked to the state of cells. Together with the morphological changes mentioned above, the decreased elasticity (increased Young's moduli) and surface adhesion were regarded as the biomechanical cues of the cells in response to the HG treatments [54, 55]. Our results demonstrated similar morphological and mechanical alterations on cells caused by HG-induced sEVs but to different extents. This phenomenon was likely due to the sources and capabilities of HG-induced sEVs that enabled them to elicit specific cellular responses similar to direct HG stimulation. sEVs delivered the HG injury-related signals and mediated the recipient cells through intercellular crosstalks.

The cellular mechanical properties under direct HG and indirect HG-induced sEV stimulations were compared to evaluate the indirect effect of HG through sEV mediation. In our previous work (Ref. 38), HG treatment for 72 h increased the average Young's modulus by over 70%, which was higher than the 26.2% recorded for the cells treated with HG-induced sEVs. This finding indicated that the direct HG stimulation resulted in a more significant change in the cellular elasticity compared with the indirect stimulation. In terms of surface adhesion, the reduction caused by the direct HG stimulation was only 5.9%, which was smaller than the 36.8% caused by the indirect HG-induced sEVs. In short, HG and indirect HG-induced sEV stimulations caused consistent mechanical trends, suggesting that both treatments induced the same physiological changes in HK-2 cells. However, differences existed in the variations of the cellular elasticity and adhesion, which could be related to the differences between glucose–cell and sEV–cell interactions.

4 Summary

This work investigated the morphologies and biomechanics of HK-2 cells responding to HG-induced sEVs via AFM-based single-cell force microscopy in air and liquid. Results showed that treatment with increasing sEV concentrations induced the morphological transformations of decreased cellular elasticity and surface adhesion. Thus, the indirect role of HG-induced sEVs in transmitting HG injury between cells was confirmed. The differences between the two stimulations were also studied by comparing the induced biomechanical changes. This work provides new insights into the research into cellular injury.

Supplementary Information The online version contains supplementary material available at https://doi.org/10.1007/s41871-023-00214-5.

Acknowledgements This study was supported by National Natural Science Foundation Program of China (No. 62175020), EU H2020 Program (ENSIGN No. 101086226), Jilin Provincial Science and Technology Program (Nos. 20210101038JC, 2020C022-1, 20190201287JC and 20190702002GH), Jilin Provincial Education Department (JJKH20220781KJ), and "111" Project of China (D17017). This work was also partly supported by Changli Nano Biotechnology (China) and China Scholarship Council (CSC, No.202007585007).

Author contributions All authors read and approved the final manuscript.

Availability of data and materials The authors declare that all data supporting the findings of this study are available within the article.

Declarations

Conflict of interest The authors declare that they have no conflicts of interest.

References

1. Negahdaripour M, Owji H, Eskandari S, Zamani M, Vakili B, Nezafat N (2021) Small extracellular vesicles (sEVs): Discovery, functions, applications, detection methods and various engineered forms. Exp Opin Biol Ther 21(3):371–394
2. Yurtsever A, Yoshida T, Badami Behjat A, Araki Y, Hanayama R, Fukuma T (2021) Structural and mechanical characteristics of

exosomes from osteosarcoma cells explored by 3D-atomic force microscopy. Nanoscale 13(13):6661–6677
3. Thery C, Zitvogel L, Amigorena S (2002) Exosomes: composition, biogenesis and function. Nat Rev Immunol 2:569–579
4. Sharma S, Gillespie BM, Palanisamy V, Gimzewski JK (2011) Quantitative nanostructural and single-molecule force spectroscopy biomolecular analysis of human-saliva-derived exosomes. Langmuir 27:14394–14400
5. Pegtel DM, Gould SJ (2019) Exosomes. Annu Rev Biochem 88:487–514
6. Pokharel D, Wijesinghe P, Oenarto V, Lu JF, Sampson DD, Kennedy BF, Wallace VP, Bebawy M (2016) Deciphering cell-to-cell communication in acquisition of cancer traits: Extracellular membrane vesicles are regulators of tissue biomechanics. Omics J Integr Biol 20(8):462–469
7. Möller A, Lobb RJ (2020) The evolving translational potential of small extracellular vesicles in cancer. Nat Rev Cancer 20:697–709
8. Liu Y, Xia YQ, Smollar J, Mao WJ (1876) Wan Y (2021) The roles of small extracellular vesicles in lung cancer: Molecular pathology, mechanisms, diagnostics, and therapeutics. Biochimica Biophysica Acta (BBA) Rev Cancer 1:188539
9. Ramanathan S, Shenoda BB, Lin ZC, Alexander GM, Huppert A, Sacan A, Ajit SK (2019) Inflammation potentiates miR-939 expression and packaging into small extracellular vesicles. J Extracellular Vesicles 8(1):1650595
10. Bardi GT, Al-Rayan N, Richie JL, Yaddanapudi K, Hood JL (2019) Detection of inflammation-related melanoma small extracellular vesicle (sEV) mRNA content using primary melanocyte sEVs as a reference. Int J Mol Sci 20:1235
11. Piszczatowska K, Czerwaty K, Cyran AM, Fiedler M, Ludwig N, Brzost J, Szczepański MJ (2021) The emerging role of small extracellular vesicles in inflammatory airway diseases. Diagnostics 11(2):222
12. Crewe C, Scherer PE (2022) Intercellular and interorgan crosstalk through adipocyte extracellular vesicles. Rev Endocr Metab Disord 23:61–69
13. James-Allan LB, Rosario FJ, Barner K et al (2020) Regulation of glucose homeostasis by small extracellular vesicles in normal pregnancy and in gestational diabetes. FASEB J 34(4):5724–5739
14. Lu YK, Wang LF, Zhang MT, Chen ZP (2022) Mesenchymal stem cell-derived small extracellular vesicles: a novel approach for kidney disease treatment. Int J Nanomed 17:3603–3618
15. Thongboonkerd V (2020) Roles for exosome in various kidney diseases and disorders. Front Pharmacol 10:1655
16. Feng Y, Liu BC, Lee K, He JC (2021) A novel mechanism of regulation for exosome secretion in the diabetic kidney. Diabetes 70(7):1440–1442
17. Zhou X, Liu RH, Duan SB, Huang GX, Ye Y, Kong Y (2016) High glucose enhances oxLDL-induced apoptosis in human renal proximal tubular epithelial cells largely via inducing lectin-like ox-LDL receptor-1. Pharmacology 98(1–2):20–28
18. Mesarosova L, Ochodnicky P, Leemans JC, Florquin S, Krenek P, Klimas J (2017) High glucose induces HGF-independent activation of Met receptor in human renal tubular epithelium. J Recept Signal Transduction 37:535–542
19. He T, Guan X, Wang S, Xiao TL, Yang K, Xu XL, Wang JP, Zhao JH (2015) Resveratrol prevents high glucose-induced epithelial–mesenchymal transition in renal tubular epithelial cells by inhibiting NADPH oxidase/ROS/ERK pathway. Mol Cell Endocrinol 402:13–20
20. Dou L, Jourde-Chiche N (2019) Endothelial toxicity of high glucose and its by-products in diabetic kidney disease. Toxins (Basel) 11(10):578
21. Vallon V (2020) Glucose transporters in the kidney in health and disease. Pflugers Arch Eur J Physiol 472(9):1345–1370
22. Liu X, Miao JH, Wang C et al (2020) Tubule-derived exosomes play a central role in fibroblast activation and kidney fibrosis. Kidney Int 97(6):1181–1195
23. Guan H, Peng R, Mao LK, Fang F, Xu B, Chen M (2020) Injured tubular epithelial cells activate fibroblasts to promote kidney fibrosis through miR-150-containing exosomes. Exp Cell Res 392(2):112007
24. Krause M, Rak-Raszewska A, Naillat F et al (2018) Exosomes as secondary inductive signals involved in kidney organogenesis. J Extracellular Vesicles 7(1):1422675
25. Ji C, Zhang J, Zhu Y et al (2020) Exosomes derived from hucMSC attenuate renal fibrosis through CK1δ/β-TRCP-mediated YAP degradation. Cell Death Dis 11:327
26. Wu XM, Gao YB, Cui FQ, Zhang N (2016) Exosomes from high glucose-treated glomerular endothelial cells activate mesangial cells to promote renal fibrosis. Biol Open 5(4):484–491
27. Wu XM, Gao YB et al (2017) Exosomes from high glucose-treated glomerular endothelial cells trigger the epithelial-mesenchymal transition and dysfunction of podocytes. Sci Rep 7:9371
28. Borges FT, Melo SA, Özdemir BC et al (2013) TGF-β1-containing exosomes from injured epithelial cells activate fibroblasts to initiate tissue regenerative responses and fibrosis. J Am Soc Nephrol 24(3):385–392
29. Musto M, Parisse P, Pachetti M, Memo C et al (2021) Shedding plasma membrane vesicles induced by graphene oxide nanoflakes in brain cultured astrocytes. Carbon 176:458–469
30. Li M, Xi N, Wang YC, Liu LQ (2021) Atomic force microscopy for revealing micro/nanoscale mechanics in tumor metastasis: from single cells to microenvironmental cues. Acta Pharmacol Sin 42(3):323–339
31. Rianna C, Radmacher M (2016) Cell mechanics as a marker for diseases: Biomedical applications of AFM. AIP Conf Proc 1760:020057
32. Garcia R (2020) Nanomechanical mapping of soft materials with the atomic force microscope: methods, theory and applications. Chem Soc Rev 49:5850–5884
33. Pi J, Cai JY (2019) Cell topography and its quantitative imaging by AFM. Mol Biol 1886:99–113
34. Li M, Dang D, Liu LQ, Xi N, Wang YC (2017) Atomic force microscopy in characterizing cell mechanics for biomedical applications: A review. IEEE Trans Nanobiosci 16(6):523–540
35. Siamantouras E, Hills CE, Squires PE, Liu KK (2016) Quantifying cellular mechanics and adhesion in renal tubular injury using single cell force spectroscopy. Nanomedicine 12(4):1013–1021
36. Thoelking G, Reiss B, Wegener J, Oberleithner H, Pavenstaedt H, Riethmuller C (2010) Nanotopography follows force in TGF-beta1 stimulated epithelium. Nanotechnology 21(26):265102
37. Chtcheglova LA, Ohlmann A, Boytsov D, Hinterdorfer P, Priglinger SG, Priglinger CS (2020) Nanoscopic approach to study the early stages of epithelial to mesenchymal transition (EMT) of human retinal pigment epithelial (RPE) cells in vitro. Life (Basel) 10(8):128
38. Yang F, Wang JJ, Qu KG, Yang X et al (2020) Dynamic mechanics of HK-2 cell reaction to HG stimulation studied by atomic force microscopy. Anal Methods 12(42):5055–5060
39. Sharma S, Rasool HI, Palanisamy V, Mathisen C et al (2010) Structural-mechanical characterization of nanoparticle exosomes in human saliva, using correlative AFM, FESEM, and force spectroscopy. ACS Nano 4(4):1921–1926
40. Shao HL, Im H, Castro CM, Breakefield X, Weissleder R, Lee H (2018) New technologies for analysis of extracellular vesicles. Chem Rev 118(4):1917–1950
41. Bellotti R, Picotto GB, Ribotta L (2022) AFM measurements and tip characterization of nanoparticles with different shapes. Nanomanuf Metrol 5:127–138

42. Krieg M, Fläschner G, Alsteens D, Gaub BM et al (2019) Atomic force microscopy-based mechanobiology. Nat Rev Phys 1:41–57
43. Kazantseva J, Ivanov R, Gasik M, Neuman T, Hussainova I (2018) Graphene-augmented nanofiber scaffolds trigger gene expression switching of four cancer cell types. ACS Biomater Sci Eng 4:1622–1629
44. Dogterom M, Koenderink GH (2019) Actin-microtubule crosstalk in cell biology. Nat Rev Mol Cell Biol 20(1):38–54
45. Antonio PD, Lasalvia M, Perna G, Capozzi V (2012) Scale-independent roughness value of cell membranes studied by means of AFM technique. Biochem Biophys Acta 1818:3141–3148
46. Altschuler SJ, Wu LF (2010) Cellular heterogeneity: do differences make a difference? Cell 141(4):559–563
47. Shin JH, Kim KM, Jeong JU, Shin JM et al (2019) Nrf2-heme oxygenase-1 attenuates high-glucose-induced epithelial-to-mesenchymal transition of renal tubule cells by inhibiting ROS-mediated PI3K/Akt/GSK-3β signaling. J Diabetes Res 2019:2510105
48. Lu Q, Chen YB, Yang H, Wang WW, Li CC, Wang L, Wang J, Du L, Yin XX (2019) Inactivation of TSC1 promotes epithelial-mesenchymal transition of renal tubular epithelial cells in mouse diabetic nephropathy. Acta Pharmacol Sin 40(12):1555–1567
49. Kwon J, Cho H (2023) Nanomechanical characterization of bone quality depending on tissue age via bimodal atomic force microscopy. Nanomanuf Metrol 6:30
50. Wang HX, Zhang H, Da B et al (2021) Mechanomics biomarker for cancer cells unidentifiable through morphology and elastic modulus. Nano Lett 21(3):1538–1545
51. Rheinlaender J, Dimitracopoulos A, Wallmeyer B et al (2020) Cortical cell stiffness is independent of substrate mechanics. Nat Mater 19:1019–1025
52. Norman MDA, Ferreira SA, Jowett GM, Bozec L, Gentleman E (2021) Measuring the elastic modulus of soft culture surfaces and three-dimensional hydrogels using atomic force microscopy. Nat Protoc 16(5):2418–2449
53. Viljoen A, Mathelié-Guinlet M, Ray A, Strohmeyer N et al (2021) Force spectroscopy of single cells using atomic force microscopy. Nat Rev Methods Primers 1:63
54. O'Connor JW, Gomez E (2014) Biomechanics of TGFβ-induced epithelial-mesenchymal transition: implications for fibrosis and cancer. Clin Transl Med 3(1):e23
55. Siamantouras E, Hills CE, Liu KK, Squires PE (2020) Examining cell-cell interactions in the kidney using AFM single-cell force spectroscopy. Diabetic Nephropathy 2067:189–201

Fan Yang She is currently a PhD student in Changchun University of Science and Technology. Her research interest is cell mechanics and nano measurement technology.

Jiajia Wang She is a research assistant at Changchun University of Science and Technology. She mainly focuses on the application of nanodetection and nanomanipulation technology in biomedicine.

Tuoyu Ju She is currently a PhD student in Changchun University of Science and Technology. Her research interest is the biological application of nano measurement and manufacturing.

Shuwei Wang He is currently the deputy director of thoracic surgery doctor in Affiliated Hospital of Jilin Medical University. His research is in the fields of lung cancer and the surgical treatment.

Kaige Qu She is a research assistant at Changchun University of Science and Technology. She mainly focuses on the application of nanodetection and nanomanipulation technology in cellular research.

Zhengxun Song He is currently a professor at Changchun University of Science and Technology. His work focuses on nanomanipulation, nanomanufacturing and systems, and optical & wireless communications.

Yujuan Chen She is currently an associate professor at Changchun University of Science and Technology. She does the research on single-cell detection, drug development and drug efficacy evaluation.

Zuobin Wang He is a professor and the director of International Research Centre for Nano Handling and Manufacturing of China, in Changchun University of Science and Technology. His research is in the fields of laser nanomanufacturing, robot nanomanipulation and nanomeasurement technology.